PFC/JA-89-27

Achievement of Second Stability by Means of Lower Hybrid Current Drive

P. T. Bonoli, M. Porkolab, D. T. Blackfield,
R. S. Devoto, M. E. Fenstermacher

Plasma Fusion Center
Massachusetts Institute of Technology
Cambridge, MA 02139

June, 1989

This paper submitted to Nuclear Fusion.

This work was supported by the U. S. Department of Energy Contract No. DE-AC02-78ET51013. Reproduction, translation, publication, use and disposal, in whole or in part by or for the United States government is permitted.

Achievement of Second Stability by Means of Lower Hybrid Current Drive

P. T. Bonoli and M. Porkolab
PLASMA FUSION CENTER, MIT, Cambridge, MA 02139
D. T. Blackfield
TRW/LLNL, Redondo Beach, CA 90278
R. S. Devoto and M. E. Fenstermacher
LLNL, Livermore, CA 94550

Abstract

It is shown that radial profiles of the safety factor q(r), necessary to access the so-called "second stability" regime in shaped, low aspect ratio tokamaks, can be achieved via off-axis lower hybrid current drive (LHCD). In order to accurately model the required current profiles, our previous simulation code for LHCD has been extended to noncircular equilibria and combined with an MHD equilibrium solver. As a particular example, results will be presented for Versator Upgrade tokamak parameters.

I. Introduction

It has been shown /1,2/ that for low aspect ratio ($R_o/a = 3$) shaped, tokamak equilibria with safety factor in the range $2 \lesssim q(\psi) \lesssim 7$, a sequence of MHD equilibria exist which allow a stable path to a high beta operating regime. Access to this region of the so-called "second stability regime" would greatly improve the operating space for D-T fusion reactors, and would allow operation with advanced fuels such as D-^3He /3/. Furthermore, it would make steady state reactor operation (ITER) more attractive owing to an increase in the bootstrap current at high values of $\epsilon\beta_p$. In this LETTER, it is shown that the required $q(\psi)$ profiles, in particular $q_o > 1$, can be achieved via off-axis lower hybrid current drive (LHCD). Specifically, it is shown that for parameters characteristic of the entrance to the second stability regime in the proposed Versator Upgrade device /4/ [$R_o/a = 3$, elongation $\kappa = 1.4$, triangularity $\delta = 0.3$, $n_{eo} = 3 \times 10^{19} m^{-3}$, $B_\phi = 1$ T, $I_p = 150$ kA, $T_{eo} \simeq T_{io} \lesssim 2$ keV], the required profiles of the safety factor with $q_o \gtrsim 2$, $q(a) \simeq 7$, $q_o \lesssim q(\psi) \lesssim q(a)$, can easily be achieved via LHRF current generation combined with ohmic currents. The required RF power is $P_{LH} \lesssim 0.3$ MW at $f_o = 2.45$ GHz and $I_{RF} \simeq 75$ kA, while $I_{OH} \simeq 75$ kA. The combined ohmic-LHRF currents give the required $q(\psi)$ profiles to enter the second stability regime. These results can easily be extended for a completely RF driven operation using additional RF systems and antennas, and for combined neutral beam injection(NBI)-RF systems for steady state reactor operation in the second stability regime. In order to accurately model this RF current generation, our previous LHCD simulation model /5/ has been modified for noncircular equilibria and added to a code which self-consistently computes free or fixed boundary MHD equilibria /6/ and current generated by neutral beams /7/, ohmic electric fields and bootstrap effects /8,9/.

The plan of this paper is as follows. The combined MHD solver and LHCD package is described in Sec. II, model results are presented in Sec. III, and conclusions are given in Sec. IV.

II. Model Calculation

Free boundary MHD equilibria are obtained by solving the Grad-Shafranov equation /10/ using a source term which includes ohmic (J_{OH}), lower hybrid (J_{RF}), bootstrap (J_{BS}), and neutral beam (J_{NB}) driven currents:

$$\Delta^*\psi = -\mu_o R^2 \frac{d}{d\psi} p(\psi) - F(\psi)\frac{dF(\psi)}{d\psi}, \tag{1a}$$

$$\Delta^*\psi = R\frac{\partial}{\partial R}\left(\frac{1}{R}\frac{\partial \psi}{\partial R}\right) + \frac{\partial^2 \psi}{\partial z^2}, \tag{1b}$$

$$F\frac{dF}{d\psi} = -\mu_o \left[F^2 \frac{d}{d\psi} p(\psi) + F\langle J_\parallel B \rangle \right] / \langle B^2 \rangle. \qquad (1c)$$

Here, ψ is the poloidal flux function, $F = RB_t$ is the toroidal function, B_t is the toroidal magnetic field, $R\underline{B} = \underline{\nabla}\psi \times \underline{e}_\phi + F\underline{e}_\phi$, $p(\psi)$ is a specified pressure profile, $\langle\rangle$ denotes a flux surface average, $R = (x^2 + y^2)^{1/2}$ is the major radial position (measured in the equatorial plane of the tokamak), and $J_\parallel = J_{OH} + J_{RF} + J_{BS} + J_{NB}$ is the total current density (along $\underline{B}$). In the present work only the ohmic and LHRF current densities are considered (i.e., $J_{NB} = J_{BS} = 0$). The iteration procedure used to solve Eq. (1) is started by first assuming that $J_{RF} = 0$ and the plasma current is purely ohmic, i.e., $J_{OH} = E_\parallel \eta_\parallel$ and $E_\parallel$ is adjusted so that the total plasma current $I_p = \int J_\parallel(\psi) dA(\psi)$ is equal to a specified value. Equation (1) is then solved to obtain a first approximation to the MHD equilibrium and the LHRF current is calculated based on this new MHD equilibrium. $E_\parallel$ is again adjusted to keep I_p constant and the Grad-Shafranov equation is solved a second time using the new source term. This process is repeated until the MHD equilibrium and J_{RF} no longer change. Typically, five to ten iterations between the MHD solver and the LHCD code are required in order to obtain convergence.

The LHCD package has been described in detail in Ref. 5. The calculation has been extended to noncircular geometry by integrating the ray equations in cartesian geometry,

$$\frac{d\underline{x}}{dt} = -\frac{\partial\epsilon/\partial\underline{k}}{\partial\epsilon/\partial\omega}, \qquad (2a)$$

$$\frac{d\underline{k}}{dt} = +\frac{\partial\epsilon/\partial\underline{x}}{\partial\epsilon/\partial\omega}, \qquad (2b)$$

where $\underline{x} = (x,y,z)$, $\underline{k} = (k_x, k_y, k_z)$, (x,y) lie in the equatorial plane of the tokamak, and z is perpendicular to the equatorial plane. The LH dispersion relation $[\epsilon(\underline{x}, \underline{k}, \omega) = 0]$ includes electromagnetic and thermal effects. The plasma quantities, $n_e(\psi)$, $T_e(\psi)$, $T_i(\psi)$, $\underline{B}(R, \psi)$ and their spatial derivatives are given in cartesian coordinates by a bi-cubic spline interpolation of the equilibrium results of the MHD solver.

A parallel velocity Fokker Planck calculation /5/ is carried out on each ψ surface in the plasma (where ψ labels a magnetic surface). The calculation is relativistically correct (i.e., $p_\parallel = \gamma m_e v_\parallel$), includes the effect of finite electron tail confinement (τ_L), an effective perpendicular electron temperature due to pitch angle scattering ($T_\perp \geq T_e$), but ignores the effect of the parallel DC electric field ($E_\parallel$). The quasilinear diffusion coefficient due to the RF waves, $D_{RF}(p_\parallel, \psi)$ is consistent with the local wave amplitude and spatial damping rates. In the

calculations presented here, we assume $T_\perp \cong 5 \times T_e$, $\tau_L = \tau_o \gamma^3$, and $\tau_o \sim \tau_E \sim$ 8.1 ms for the parameters given below.

III. Model Results

The parameters used to study LHRF current profile control are typical of the proposed Versator Upgrade device /4/ where a = 0.3 m, R_o = 0.9 m, B_{to} = 1.0 T, I_p = 150 kA, κ = 1.4, δ = 0.3, Z_{eff} = 1.5, hydrogen gas, $n_{eo} = 3 \times 10^{19} m^{-3}$, and $T_{eo} = T_{io}$ = (1.5 − 2.0) keV. The plasma profiles were chosen to be $n_e(\psi) = n_{eo}(1-\psi_n)^{\gamma_n}$, $T_\alpha(\psi) = T_{\alpha o}(1-\psi_n)^{\gamma_{t\alpha}}$, γ_n = 1.0, $\gamma_{te} = \gamma_{ti}$ = 1.25, $\psi_n = (\psi - \psi_a)/(\psi_o - \psi_a)$, $\psi_a = \psi(a)$, and $\psi_o \equiv \psi(0)$. The pressure profile is determined from $p(\psi) = n_e(\psi)[T_e(\psi) + T_i(\psi)]$. The RF parameters used were f_o = 2.45 GHz, $P_{LH} \leq$ 500 kW, and a superposition of the RF power spectra shown in Fig. 1 for relative waveguide phasings of $\Delta\phi = \pi/2$ and $2\pi/3$. The relevant parameters for LH wave accessibility are $(\omega_{pe}/\omega_{ce})^2$ = 3.09 and $n_{\parallel acc}$ = 3.73, where $n_{\parallel acc}$ is the minimum value of parallel refractive index required for wave accessibility to the plasma center.

The results of LHRF current profile control at different RF powers are summarized in Table I ($T_{eo} = T_{io}$ = 1.5 keV) and in Table II ($T_{eo} = T_{io}$ = 2.0 keV). The current drive figure of merit used in these tables is defined as $\eta_{CD} \equiv \bar{n}_e(10^{20} m^{-3}) I_{RF}(kA) R_o(m)/P_{LH}(kW)$, where $\bar{n}_e$ is the line-averaged density, $\beta_p = \langle p(\psi)\rangle_v / (\langle B_\theta \rangle^2 / 2\mu_o)$ is the volume average poloidal beta, and $\epsilon = a/R_o$ is the inverse aspect ratio.

Although $q_o \approx 2.0$ at T_{eo} = 1.5 keV (Table I), the profiles of $q(\psi)$ are hollow with minima of $q_{min} \simeq$ 1.3 - 1.4 at $\psi_n \simeq 0.2$. This is to be contrasted with the results obtained for T_{eo} = 2.0 keV (Table II) where $q_o > 2$ and $q(\psi) >$ 2 persists for $0 \leq \psi_n \leq 1$. The reason for $q(\psi) \lesssim 2$ at the higher temperature is that the RF current profile is broader and peaked farther from the plasma axis as T_{eo} increases (owing to the stronger electron Landau damping of the lower hybrid waves). Consequently, a "shoulder" is created in the total current density profile ($J_\parallel$) by adding RF current off-axis. Then, for a fixed total current (I_p), the central values of $J_\parallel$ are constrained to be low, forcing $q(\psi)$ to remain high. Acceptable $q(\psi)$ profiles could be obtained even in the case of T_{eo} = 1.5 keV, however, the $n_\parallel$ spectrum of the launchers would have to be increased.

In the cases shown in Tables I and II, about 85% of the injected RF power is absorbed resonantly due to electron Landau damping. The remaining RF power at $n_\parallel < n_{\parallel acc} \cong 3.7$ is not accessible to the plasma core (see Fig. 1), even after multiple radial reflections at the plasma edge. It is also interesting to note that the fraction of injected power lost due to electron tail losses (P_L) is negligible in all cases with $P_L \lesssim 0.04 P_{LH}$. This small tail loss is consistent with the rapid

thermalization and negligible spatial diffusion of fast electrons. Although the values of $\epsilon\beta_p$ in Table II are rather modest ($\epsilon\beta_p \simeq$ 0.5-0.6), they are very near the critical value found in Ref. 2 ($\epsilon\beta_p \geq$ 0.6-0.7) for which further increases in beta will result in entering the second stability regime.

Results from the T_{eo} = 2 keV case in Table II at P_{LH} = 200 kW are shown in Figs. 2(a)-2(d). Figure 2(a) is a plot of $J_{OH}(\psi)$ and $J_{RF}(\psi)$ after the fifth and final iteration between the current drive code and MHD solver. The LHRF current in this case was 53 kA and the ohmic current was 97 kA. The peak in the RF power deposition at $\psi_n \cong 0.325$ (Table II) is to be contrasted with the peak of $\psi_n = 0.1$ at T_{eo} = 1.5 keV and P_{LH} = 250 kW (Table I). The resulting $q(\psi)$ profile is shown in Fig. 2(b). The ohmic $q(\psi)$ profile ($P_{LH} = 0$) has also been shown in Fig. 2(b) for comparison (dashed line). We note that the typical single turn loop voltage required to maintain the ohmic current under the present conditions is $\sim$ 0.1 volts. The time needed to come to steady state conditions after application of the RF power is not more than 0.25 sec.

The poloidal projection of a single ray trajectory (initial $n_{\|}^{o} = 4.40$) for this case is shown in Fig. 2(c). Each tick mark along the ray path indicates a 20% decrease in the wave power due to quasilinear electron Landau damping. The electron distribution function on a flux surface near the maximum in the RF deposition ($\psi_n \cong 0.325$) is shown in Fig. 2(d), plotted as a function of parallel kinetic energy $E = m_e c^2[n_{\|}/(n_{\|}^2 - 1)^{1/2} - 1]$. It should be pointed out that the slowing down time for the fast electrons in the plateau region of Fig. 2(d) is approximately $\tau_s \lesssim 2.6 \times 10^{-3}$ sec (assuming $n_e \simeq 1.8 \times 10^{19} m^{-3}$ and E $\simeq$ 31 keV at $\psi_n = 0.325$). However, $\tau_s \ll \tau_L$ so that electrons would be expected to thermalize before spatially diffusing an appreciable distance.

IV. Conclusions

In conclusion, a powerful computational tool has been developed to study lower hybrid current profile control in self-consistent MHD equilibria. Utilizing this model, it has been shown that the $q(\psi)$ profiles [$2 \lesssim q(\psi) \lesssim 7$] necessary to access a high poloidal beta operating regime ("second stability regime") in shaped tokamak equilibria can be achieved, via off-axis LHRF current generation with $I_{RF} \lesssim 0.5 \times I_p$. This model can also be used to study current profile control and steady state operation with NBI, LH current drive, and bootstrap current generation in reactor relevant plasma regimes ($n_e \lesssim 1 \times 10^{20} m^{-3}$ and $T_e, T_i \lesssim$ 25 keV). Due to the relatively simple waveguide launcher geometry chosen here, (eight waveguide grill) a rather crude approximation to the optimal $q(\psi)$ profile was obtained. In principle, these results can be refined by using multiple waveguide launchers with more than eight radiating elements.

Acknowledgements

This work was supported by the US DOE under Contract No. DE-AC02-78ET51013 at MIT and under Contract No. W-7405-ENG-48 at LLNL.

Table I:
(Lower Hybrid Current Drive Parameters for $T_{eo} = 1.5$ keV)

P_{LH}(kW)	q_o	$\epsilon\beta_p$	I_{RF}(kA)	η_{CD}
0	1.00	0.27	0	–
250	1.92	0.32	60	0.043
375	2.15	0.32	91	0.044

Table II:
(Lower Hybrid Current Drive Parameters for $T_{eo} = 2$ keV)

P_{LH}(kW)	q_o	$\epsilon\beta_p$	I_{RF}(kA)	η_{CD}
0	0.99	0.36	0	–
200	2.27	0.53	58	0.048
250	3.14	0.60	64	0.046

References

[1] Coppi, B., Crew, G. B., Ramos, J. J., Comments Plasma Phys. Contr. Fusion 6 (1981) 109.

[2] Gerver, M. J., Kesner, J., Ramos, J. J., Phys. Fluids 31 (1988) 2674.

[3] Atzeni, S. and Coppi, B., Comments Plasma Phys. Cont. Fusion 6 (1980) 77.

[4] Porkolab, M. Bonoli, P., Chen, K. I., Coda, S., Gerver, M., et al, 12th Int. Conf. on Plasma Physics and Controlled Fusion Research (Nice, France, 1988) Paper IAEA CN-50/E-4-8.

[5] Bonoli, P. T., Englade, R. C., Phys. Fluids 29 (1986) 2937.

[6] Azumi, M., Kurita, G., Proc. 4th Int. Symp. Computing Methods in Appl. Science and Eng. (Paris, 1979) 335.

[7] Tani, K., Suzuki, M., Yamamoto, S., Azumi, M., Report JAERI-M 88-042 (1988).

[8] Devoto, R. S., Tani, K., Azumi, M., 15th Eur. Conf. Contr. Fusion and Plasma Heating, Vol. III (1988) 1055.

[9] Devoto, R. S., Blackfield, D. T., Fenstermacher, M. E., Bonoli, P. T., Porkolab, M., 16th European Conf. on Controlled Fusion and Plasma Physics, Vol. IV (1989) 1295

[10] Freidberg, J. P. in "Ideal Magnetohydrodynamics" (Plenum, NY, 1987) Ch. 6, p. 111.

Figure Captions

Fig. 1. RF power spectra for an eight waveguide, 2.45 GHz, LH launcher (grill dimensions were 0.7cm × 10cm, with adjacent guides separated by 0.1cm). Relative waveguide phasings are $\Delta\phi = \pi/3, \pi/2$, and $2\pi/3$. Results were obtained using an LH coupling code [M. Brambilla, Nucl. Fusion 16 (1976) 47].

Fig. 2. Model results for Versator Upgrade parameters ($n_{eo} = 3 \times 10^{19} m^{-3}$, $T_{eo} = T_{io}$ =2 keV, $B_{to} = 1.0$ T, $I_p = 150$ kA, and $P_{LH} = 200$ kW). (a) Current density vs. ψ. (b) q vs. ψ for $P_{LH} = 200$ kW (solid line) and for comparison $P_{LH} = 0$ (dash line). (c) Poloidal projection of ray trajectory ($n_{\|}^{0} = 4.40$). (d) Electron distribution function versus parallel kinetic energy on a flux surface ($\psi_n \cong 0.325$) near the maximum of the RF deposition profile.

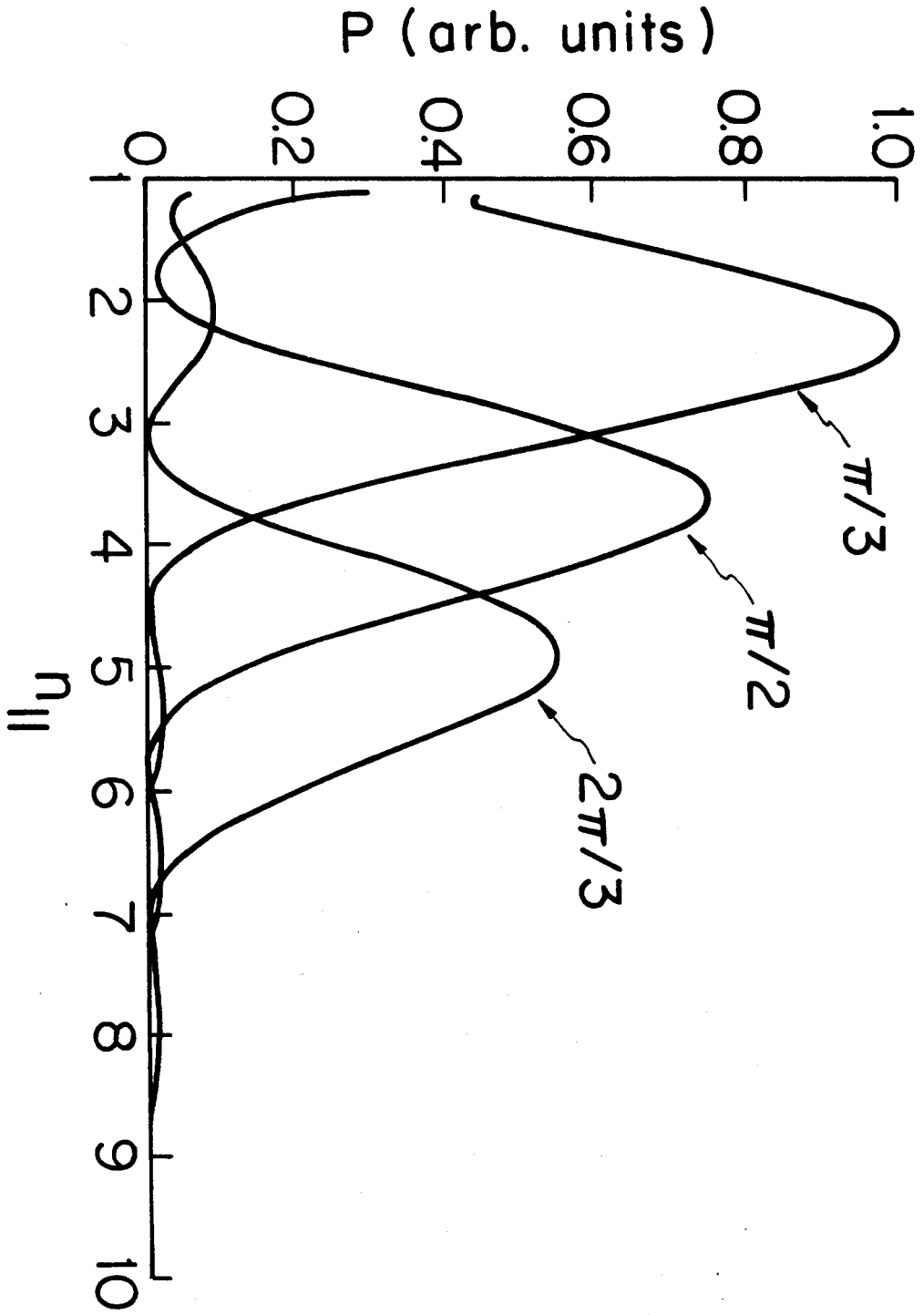
P (arb. units)
0
0.2
0.4
0.6
0.8
1.0
1
2
3
4
5
6
7
8
9
10
$n_{\parallel}$
$\pi/3$
$\pi/2$
$2\pi/3$

Figure 1

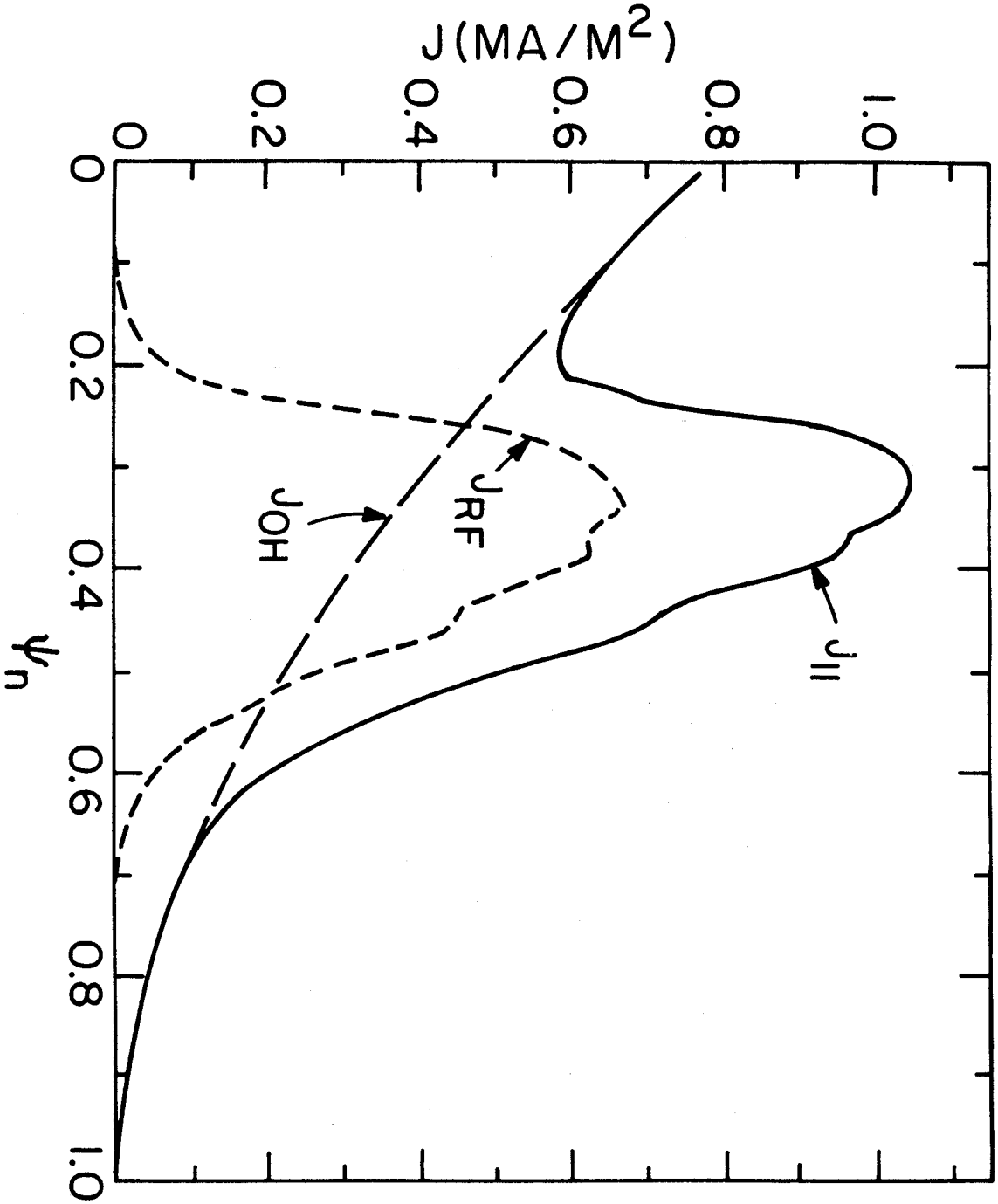

Figure 2(a)

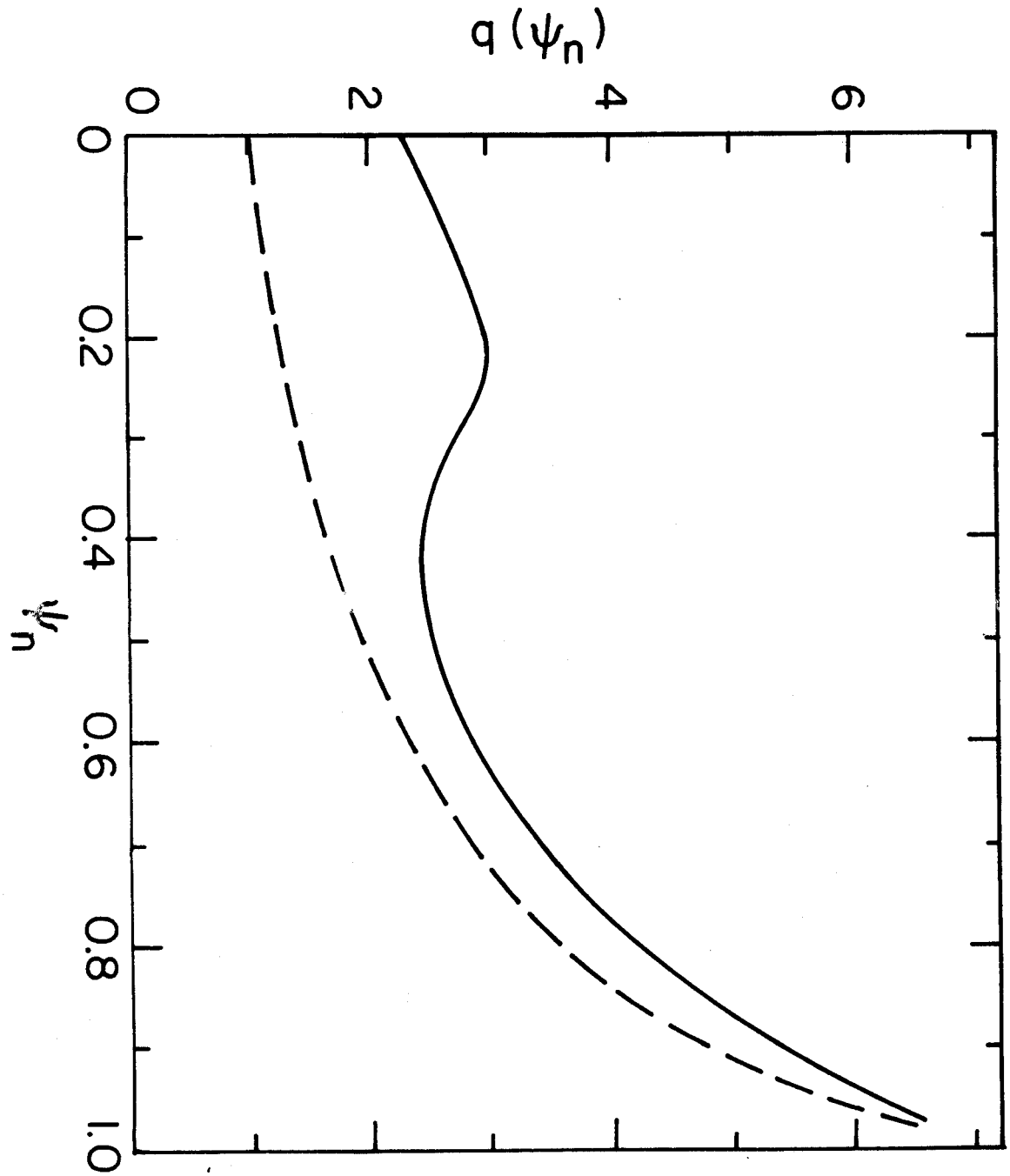

Figure 2(b)

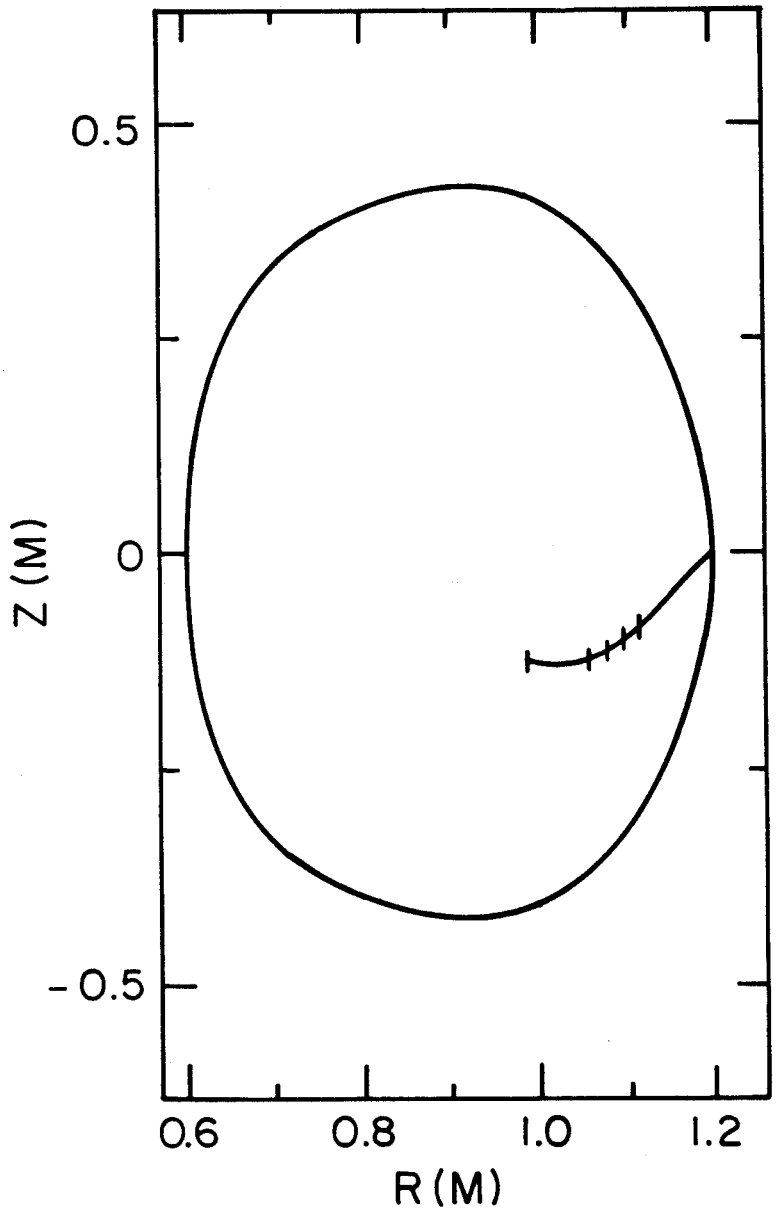

Figure 2(c)

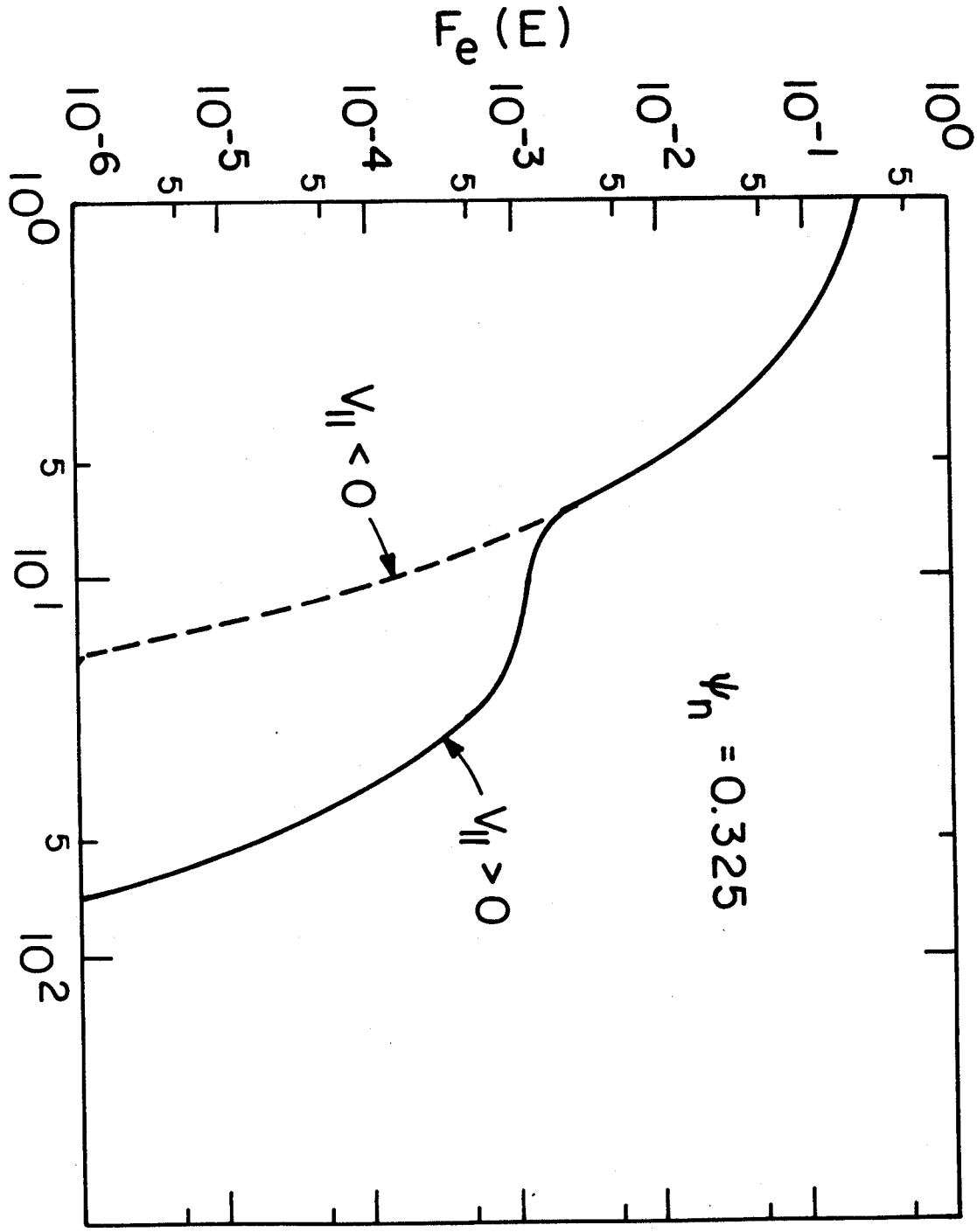
$F_e(E)$
10^{-6}
10^{-5}
10^{-4}
10^{-3}
10^{-2}
10^{-1}
10^{0}
5
10^{0}
10^{1}
10^{2}
E (keV)
$V_{\parallel} < 0$
$V_{\parallel} > 0$
$\psi_n = 0.325$

Figure 2(d)